Research Article

Christoph Holst*, Thomas Artz, and Heiner Kuhlmann

Biased and unbiased estimates based on laser scans of surfaces with unknown deformations

Abstract: The estimates based on laser scans of surfaces with unknown deformations are biased and not reproducible when changing the scanning geometry. While the existence of a bias is only disadvantageous at some applications, non-reproducible estimates are never desired. Hence, this varying bias and its origin need to be investigated – since this situation has not been examined sufficiently in the literature. Analyzing this situation, the dependence of the estimation on the network configuration is highlighted: the network configuration – studied similarly to geodetic networks – rules about the impact of the deformation.

As pointed out, this impact can be altered by manipulating the network configuration. Therefore, several strategies are proposed. These include manipulations of the least-squares adjustment as well as robust estimation. It is revealed that the reproducibility of the estimates can indeed be significantly increased by some of the proposed least-squares manipulations. However, the bias can only be significantly reduced by robust estimation.

Keywords: laser scanning, deformation, surface approximation, bias, network configuration, partial redundancies

DOI 10.1515/jag-2014-0006
Received February 20, 2014; accepted June 14, 2014.

1 Introduction

Laser scanners have become one of the most used instruments by geodetic engineers. The technical progress regarding measurement frequency, spatial resolution and accuracy lead to an increase of laser scanner applications, especially in geodetic deformation measurements, reverse engineering or general surface analysis. Dependent on this trend, the investigation of surfaces also develops from pointwise considerations to an analysis of the complete surface structure and its estimated parameters.

This great enhancement of given data bears new possibilities especially regarding the spatial resolution of measured (deformed) objects. Nevertheless, – what is often neglected when working with this great amount of point data – the measurement geometry and the configuration of adjustment are still restricted to the same rules as if working with only a limited number of observations. In this connection, the point cloud of a laser scanner can be regarded as a geodetic network. Thus, its quality regarding the accuracy and especially the reliability has to be proven similar to other geodetic networks. This should always be considered when using laser scanner point clouds for surface analysis where high accuracy is of interest.

1.1 Uncovering the varying bias

Laser scanner point clouds are often used to parameterize surfaces (e.g., [3, 13, 16]). Based on the sampled surface, functional and stochastic models are built up and their consistence is proven in some studies by, e.g., a global test or other tools to reveal mismodeling [7, 10]. Other studies analyze the scanning geometry regarding point accuracies, sampling resolution or the resulting level of detail dependent on the laser beam footprint [23, 24, 30, 33–35]. However, – what has not been addressed in previous studies sufficiently – scanned surfaces are often only known to a certain level of detail that does not characterize the surface sufficiently. Thus, unknown (local) deformations deviating from the assumed functional model might exist.

A previous study of the present paper revealed that these deformations can result in biased and non-reproducible parameter estimates when approximating scanned surfaces [15]. This bias is defined as the mean deviation of the estimated parameters from the true value; the reproducibility equals the difference between maximal and minimal variation of each parameter. While the exis-

***Corresponding Author: Christoph Holst:** Institute of Geodesy and Geoinformation, University of Bonn, Nussallee 17, 53115 Bonn, Germany, E-mail: c.holst@igg.uni-bonn.de
Thomas Artz, Heiner Kuhlmann: Institute of Geodesy and Geoinformation, University of Bonn, Nussallee 17, 53115 Bonn, Germany

tence of a bias is only disadvantageous at some applications, non-reproducible estimates are never desired.

As will be shown, this varying bias results from the scanning geometry-dependent network configuration of the adjustment. This network configuration is based upon

1. the varying sampling density that originates from the scanner-typical sampling of surfaces (Figure 1),
2. the object's geometry and
3. the observations' stochastic model.

Resulting from this network configuration, local deformations are weighted. This weight can be expressed by the partial redundancies that define the reliability of each observation in a least-squares adjustment [9]. Hence, altering the scanning geometry leads to different systematics in the partial redundancies and, thus, to non-reproducible parameter estimates. Regarding Figure 1, these statements would mean that (1) an approximation of the surface would always be biased and that (2) this bias would be different when scanning from station 2 instead of station 1.

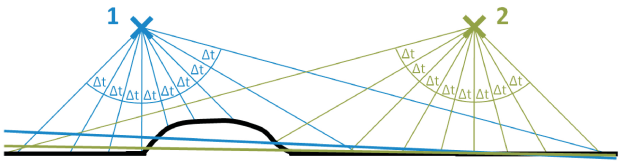

Fig. 1. Two-dimensional sketch of the sampling densities when scanning a locally deformed plane (black line) from stations 1 and 2 (crosses). The resulting estimations are differently biased (thick lines). The angular scanning resolution – that is excessively thinned here for reasons of displaying – is indicated by the increments Δt and the laser beam vectors (thin lines).

Usually, partial redundancies are used for quality control or optimization of geodetic networks (e.g., [11, 14]): low partial redundancies – implying poor reliability – as well as high ones – attesting poor cost effectiveness – should be avoided. However, their validity can be transferred to the present application. Though their individual magnitude is not of importance here due to the high redundancy in the adjustment, the spatial variation of their magnitude in the point cloud helps analyzing and justifying the results of parameter estimation.

1.2 Handling the varying bias

Non-parameterized deformations equal systematic errors in the functional model. This is an unusual situation in typical geodetic approximation problems because systematic errors are considered most times only regarding the observations, not regarding the parameterization of the surface (e.g., [16, 38]). However, the strategies for dealing with systematic errors in the observations can be tried to transfer to dealing with systematic errors in the functional model aiming at increasing reproducibility and unbiasedness. This can either be done by simply eliminating only the variation of the bias – which increases the reproducibility – or by eliminating the bias itself – which increases the reproducibility and also the unbiasedness.

As already mentioned, the network configuration that rules about the bias is based upon (1.) the sampling density, (2.) the sampled object's geometry and (3.) the stochastic model of the observations. Hence, changing the impact of either one of these aspects modifies the partial redundancies and the network configuration. This could be done by (1.) data reduction [20, 21, 26, 32, 43], (2.) balancing the adjustment [25] or (3.) insertion of spatial correlations.

Apart from modifying the least-squares adjustment, the robust estimation – usually used for dealing with gross observational errors – is also worth investigating. Here, the BIBER-estimator (Bounded Influence By Standardized Residuals [40, 41]) or the RANSAC-algorithm (Random Sample Consensus [5, 8, 37]) can be named.

1.3 Main aspects of the present study

The present study points out how local, non-parameterized deformations on a surface can impact the parameter estimation. Furthermore, strategies for dealing with this situation are given and investigated (Table 1). Both is performed by approximating a (deformed) plane based on simulated scans. Altogether, this study

- uncovers the varying bias of estimates based on laser scans of a deformed plane,
- investigates several strategies for increasing the reproducibility and the unbiasedness,
- analyzes these strategies based on the network configuration and
- shows limits of least-squares estimations regarding non-parameterized deformations.

Here, the focus is laid on investigating several modifications of a classical least-squares estimation to increase

Table 1. Strategies for increasing the reproducibility and the unbiasedness of the estimates based on laser scans of deformed surfaces.

Least-squares	Robust
Data reduction	BIBER-estimator
Insertion of spatial correlations	RANSAC-algorithm
Balancing the adjustment	

the reproducibility and the unbiasedness of the estimates. Thereby, it is analyzed how the variation of the bias and the bias itself can be minimized without detecting and eliminating the points belonging to the deformation and without parameterizing the deformation. As robust techniques are often used for dealing with gross errors, they are also investigated. They shall suggest the limits of least-squares techniques.

2 Simulating and approximating laser scans

The present section gives an overview about parameterizing a plane as well as about simulating and approximating laser scans of sampled (deformed) planes. This overview is presented here for reasons of completeness and to clarify the basics used in the following sections. However, the sophisticated reader might skip this section.

2.1 Equation of planes

A plane can be described by 4 parameters $\mathbf{p}_4 = [n_x, n_y, n_z, d]$ in three-dimensional space:

$$n_x \cdot x + n_y \cdot y + n_z \cdot z = d. \tag{1}$$

Here, n_x, n_y, n_z equal the three components of the plane's normal vector and d describes the orthogonal distance of the plane to the center of the (local) coordinate sytem $[x, y, z]$ in which the coordinates x, y, z are given [31]. Usually, the normal vector is normalized to eliminate the ambiguity in the parameter vector. Instead, the uniqueness can be achieved by dividing the distance d resulting in

$$\underbrace{\frac{n_x}{d}}_{\overline{n}_x} \cdot x + \underbrace{\frac{n_y}{d}}_{\overline{n}_y} \cdot y + \underbrace{\frac{n_z}{d}}_{\overline{n}_z} \cdot z = 1. \tag{2}$$

This is attended by a reduction of the number of parameters

$$\mathbf{p} = [\overline{n}_x, \overline{n}_y, \overline{n}_z]^T \tag{3}$$

to $u = 3$ describing a plane in three-dimensional space.

2.2 Simulating laser scans of (deformed) planes

For analyzing the bias in the approximation of deformed planes based on laser scans, several simulations are performed. They are all based on generating the laser scanner observations $\mathbf{l}$, i.e., distances s_i, vertical angles β_i and horizontal directions t_i of number $i = 1, \ldots, m$ each:

$$\mathbf{l} = [s_1, \beta_1, t_1, \ldots, s_m, \beta_m, t_m]^T. \tag{4}$$

As the observation triplets s, β, t are of number m each (number of points), the number of observation equals $n = m \cdot 3$.

The observations are based on the scanning geometry, i.e., the station of the laser scanner and the position, the orientation and the shape of the measured object. To simulate realistic observations, several aspects have to be considered: (1.) the scanning geometry has to be defined. (2.) Based on this, true laser scanner observations can analytically be calculated. (3.) Afterwards, these measurements have to be noised to gain a realistic realization of the true measurements. These steps will be explained in the following.

2.2.1 Assessing the scanning geometry

The observations of eq. (4) are given in the laser scanner coordinate system $[x, y, z]$. This varies between different simulation runs as the station of the laser scanner changes. To evaluate the effect of different laser scanner stations, the simulated plane and the position of the scanner are defined in a global coordinate system $[X, Y, Z]$ where the transformation parameters between local and global system are always known. The position, orientation and magnitude of the plane is always constant. Thus, the estimated parameters are comparable between different simulations by transforming them into the global coordinate system. The simulated global plane parameters equal

$$[n_x, n_y, n_z, d]^T = [0, 1, 0, 0]^T. \tag{5}$$

The plane's dimensions are $0m \le X \le 20m$ and $0 \le Z \le 5m$ and – resulting from eq. (5) – $Y = 0$. Figure 2 shows this plane in the global coordinate system $[X, Y, Z]$ scanned from station no. 1. As can be seen in Figure 3, this station varies during the simulation between no. 1–5.

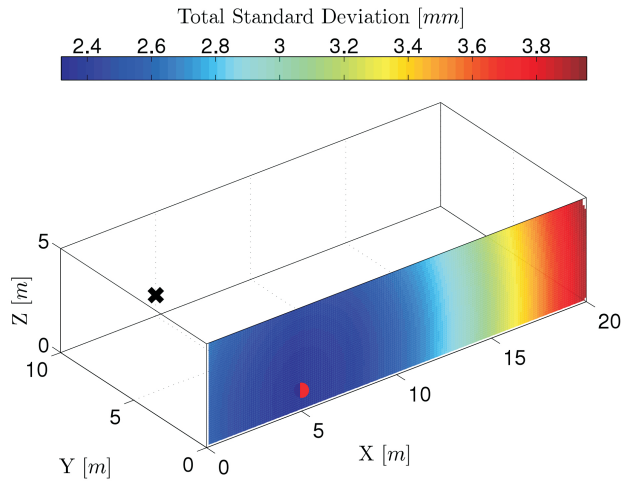

Fig. 2. Simulated sampled plane from station no. 1 (black cross); projection of station in plane (red dot) and total standard deviation $\sigma_{xyz,i}$ (eq. 9).

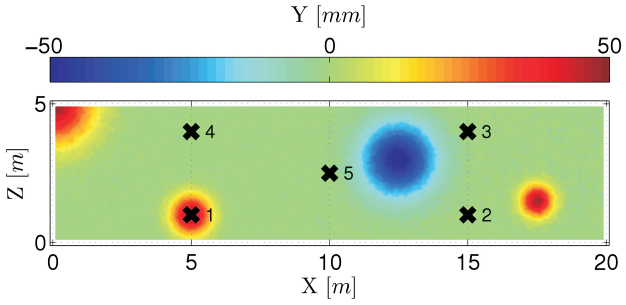

Fig. 3. Simulated plane that is scanned by the five stations no. 1–5 (crosses, projected in XZ-plane) containing four deformations indicated by deviations in Y.

2.2.2 Calculating observations

By defining the origin and orientation of the local laser scanner coordinate system $[x, y, z]$ inside the global one, corresponding observations can be simulated. These observations are generated similar to the real scanning procedure by sampling the surface with constantly increasing vertical angle β and horizontal direction t: $\beta_i = \beta_1 + i \cdot \Delta\beta$ and $t_i = t_1 + i \cdot \Delta t$.

The corresponding distances s_i are gained by analytical geometry. They equal the distance between the laser scanner station and the point of intersection between the laser beam vectors – built up by horizontal and vertical angles – and the sampled surface. In case of an undeformed plane, eq. (2) is used to represent the surface and to calculate the point of intersection for each observation. If local deformations exist on the plane, the distances are calculated analytically by integrating radial basis functions representing the deformations on the plane (Figure 3) [39].

The resulting sampling points of number $i = 1, \ldots, m$ can be calculated by

$$\mathbf{x}_i = \begin{bmatrix} x \\ y \\ z \end{bmatrix}_i = \begin{bmatrix} s \cdot \sin\beta \cdot \cos t \\ s \cdot \sin\beta \cdot \sin t \\ s \cdot \cos\beta \end{bmatrix}_i . \tag{6}$$

The sampling density is not homogenous and due to the scanning geometry, i.e., the station of the laser scanner and the position, orientation and shape of the measured object. This is shown in Figure 4 as the sampling density descreases when increasing the distance to the scanner.

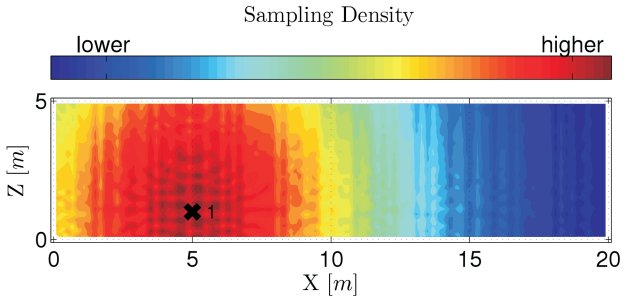

Fig. 4. Approximative sampling density of the simulated observations at station no. 1 (cross, projected in XZ-plane).

2.2.3 Noising the observations

The calculated measurements are assumed to be randomly noised, i.e., the residuals follow a Gaußian distribution, to generate realistic realizations. Thus, the simulation also integrates residuals

$$\mathbf{v} = \left[v_{s,1}, v_{\beta,1}, v_{t,1}, \ldots, v_{s,m}, v_{\beta,m}, v_{t,m}\right]^T \tag{7}$$

of number n based on the standard deviations $\sigma_{s,i} = 0.5mm + s_i \cdot 0.1mm/m$, $\sigma_\beta = 125\mu rad \approx 8mgon$ and $\sigma_t = 125\mu rad \approx 8mgon$. These errors equal typical laser scanner noise (e.g., Leica HDS6100 [22]). Thus, the covariance matrix $\boldsymbol{\Sigma}_{ll,i}$ of a single observation triplet and the one of the whole point cloud $\boldsymbol{\Sigma}_{ll}$, respectively, equal

$$\boldsymbol{\Sigma}_{ll} = \begin{bmatrix} \underbrace{\begin{bmatrix} \sigma_{s,1}^2 & & \\ & \sigma_\beta^2 & \\ & & \sigma_t^2 \end{bmatrix}}_{\boldsymbol{\Sigma}_{ll,1}} & & \\ & \ddots & \\ & & \boldsymbol{\Sigma}_{ll,m} \end{bmatrix} . \tag{8}$$

As only the main diagonal of $\boldsymbol{\Sigma}_{ll}$ is filled, no correlations are assumed to exist. Based on this, the total standard deviation of the sampling points $\mathbf{x}_i$ (eq. 6) is given by

$$\sigma_{xyz,i} = \sqrt{\sigma_{x,i}^2 + \sigma_{y,i}^2 + \sigma_{z,i}^2} \tag{9}$$

where $\sigma_{x,i}$, $\sigma_{y,i}$, $\sigma_{z,i}$ are gained by variance propagation of $\boldsymbol{\Sigma}_{ll,i}$ using eq. (6) [18]. This total standard deviation is shown in Figure 2. It is visible that the noise increases proportionally to the distances s_i based on $\sigma_{s,i}$.

2.3 Approximating laser scans

For approximating the laser scans of the (deformed) surfaces, the cost function $\mathbf{v}^T\boldsymbol{\Sigma}_{ll}^{-1}\mathbf{v}$ is minimized. This usually leads to the Gauß-Helmert model (GHM) – also known as general case of adjustment [27] – regarding the functional model of eq. (2).

This GHM can be reduced to a Gauß-Markov model (GMM) which is advantageous since the later introduced manipulations of the approximation can be implemented more straightforward in a GMM (see Secs. 4-5).

2.3.1 Gauß-Helmert model

The functional model of the GHM should equal eq. (2) instead of eq. (1) when approximating a plane to avoid the ambiguity. Furthermore, taking into account that the noised observations $\mathbf{l} + \mathbf{v}$ are incorporated in eq. (2), the functional model is set up as

$$\begin{aligned} f(\mathbf{l}+\mathbf{v}, \mathbf{p}) = {} & \overline{n}_x \cdot (s + v_s) \cdot \sin(\beta + v_\beta) \cdot \cos(t + v_t) \\ & + \overline{n}_y \cdot (s + v_s) \cdot \sin(\beta + v_\beta) \cdot \sin(t + v_t) \\ & + \overline{n}_z \cdot (s + v_s) \cdot \cos(\beta + v_\beta) - 1 \\ = {} & 0. \end{aligned} \tag{10}$$

The stochastic model is based on the covariance matrix of the observations $\boldsymbol{\Sigma}_{vv} = \boldsymbol{\Sigma}_{ll}$ of eq. (8). The further explanations regarding the strict solution of the nonlinear GHM are given in [15, 27, 28] but are recapitulated here for reasons of completeness.

Because the model of eq. (10) is nonlinear, parameter updates $\Delta\hat{\mathbf{p}}$ with $\hat{\mathbf{p}} = \Delta\hat{\mathbf{p}} + \hat{\mathbf{p}}_0$ are estimated iteratively – where $\hat{\mathbf{p}}_0$ are the estimated parameters of the last iteration – until convergence is reached. The linearized functional model equals

$$\mathbf{B} \cdot (\mathbf{v} - \hat{\mathbf{v}}) + \mathbf{A} \cdot (\mathbf{p} - \hat{\mathbf{p}}_0) + f(\mathbf{l} + \hat{\mathbf{v}}, \hat{\mathbf{p}}_0) = \mathbf{0} \tag{11}$$

when introducing approximate residuals $\hat{\mathbf{v}}$ that are updated in each iteration [28]. Here, the Jacobian matrices, i.e., design matrix $\mathbf{A}$ and condition matrix $\mathbf{B}$, are evaluated at the estimated parameters $\hat{\mathbf{p}}_0$ as well as at the iteratively approximated observations $\mathbf{l} + \hat{\mathbf{v}}$:

$$\mathbf{A} = \left.\frac{\partial f}{\partial \mathbf{p}}\right|_{\mathbf{l}+\hat{\mathbf{v}}, \hat{\mathbf{p}}_0} \quad ; \quad \mathbf{B} = \left.\frac{\partial f}{\partial \mathbf{l}}\right|_{\mathbf{l}+\hat{\mathbf{v}}, \hat{\mathbf{p}}_0}. \tag{12}$$

Based on eqs. (11) and (12), by defining the vector of discrepancies as

$$\mathbf{w} = -\mathbf{B} \cdot \hat{\mathbf{v}} + f(\mathbf{l} + \hat{\mathbf{v}}, \hat{\mathbf{p}}_0) \tag{13}$$

and the Lagrange multipliers as $\mathbf{k}$, the normal equations

$$\begin{bmatrix} \boldsymbol{\Sigma}_{\overline{ll}} & \mathbf{A} \\ \mathbf{A}^T & \mathbf{0} \end{bmatrix} \cdot \begin{bmatrix} \mathbf{k} \\ \Delta\hat{\mathbf{p}} \end{bmatrix} = \begin{bmatrix} -\mathbf{w} \\ \mathbf{0} \end{bmatrix} \tag{14}$$

can be built up, where $\mathbf{B}\boldsymbol{\Sigma}_{ll}\mathbf{B}^T$ is substituted by

$$\boldsymbol{\Sigma}_{\overline{ll}} = \mathbf{B}\boldsymbol{\Sigma}_{ll}\mathbf{B}^T. \tag{15}$$

The normal equations (14) are used to iteratively estimate the parameter updates $\Delta\hat{\mathbf{p}}$, the residuals $\hat{\mathbf{v}}$ and finally $\hat{\mathbf{p}}$ and $\boldsymbol{\Sigma}_{\hat{p}\hat{p}}$ [27].

2.3.2 Reduction to a Gauß-Markov model

The GHM can be reduced to a GMM [6, 18]. This reduction is strict and, thus, reversible [27]. As requirement for the transformation, the rank of $\mathbf{B}$ (eq. 12) needs to be full: $\text{rank}(\mathbf{B}) = m$. However, this is always fulfilled regarding laser scanner measurements as no observation is performed twice or more often. Since the later explained manipulations of the approximation are defined in a GMM, the reduction to a GMM is explained in the following.

The reduction to the GMM is based on substituting

$$\overline{\mathbf{v}} = \mathbf{B}\mathbf{v}. \tag{16}$$

This leads to the already described variance propagation from $\boldsymbol{\Sigma}_{ll} = \boldsymbol{\Sigma}_{vv}$ to $\boldsymbol{\Sigma}_{\overline{ll}}$ (eq. 15). By defining the reduced substituted observations $\Delta\bar{\mathbf{l}} = -\mathbf{w}$, the parameter updates and their covariance matrix are estimated by

$$\Delta\hat{\mathbf{p}} = \left(\mathbf{A}^T\boldsymbol{\Sigma}_{\overline{ll}}^{-1}\mathbf{A}\right)^{-1}\mathbf{A}^T\boldsymbol{\Sigma}_{\overline{ll}}^{-1}\Delta\bar{\mathbf{l}} \tag{17}$$

$$\boldsymbol{\Sigma}_{\hat{p}\hat{p}} = \left(\mathbf{A}^T\boldsymbol{\Sigma}_{\overline{ll}}^{-1}\mathbf{A}\right)^{-1}. \tag{18}$$

Here, the covariance matrix $\boldsymbol{\Sigma}_{\overline{ll}}$ (eq. 15) equals a main diagonal matrix since $\boldsymbol{\Sigma}_{ll}$ (eq. 8) is also a diagonal matrix. Thus, the substituted observations $\bar{\mathbf{l}}$ are not correlated similar to the original ones $\mathbf{l}$. Simultaneously, – as their number is reduced from n to m – only one single substituted observation $\bar{l}_i$ and its corresponding variance $\sigma_{\bar{l},i}^2 = \left[\boldsymbol{\Sigma}_{\overline{ll}}\right]_{i,i}$ represent the whole observation triplet $\mathbf{l}_i = [s_i, \beta_i, t_i]^T$ and its

covariance matrix $\boldsymbol{\Sigma}_{ll,i}$ of eq. (8). The same applies for the residuals $\mathbf{v}$ and their substitutions $\overline{\mathbf{v}}$ (eq. 16). Interpreted geometrically, observations and residuals are transformed to the condition space.

From the previous derivations, the estimated substituted residuals and their covariance matrix equal

$$\hat{\overline{\mathbf{v}}} = \Delta\overline{\mathbf{l}} - \mathbf{A}\Delta\hat{\mathbf{p}} \tag{19}$$

$$\boldsymbol{\Sigma}_{\hat{\overline{v}}\hat{\overline{v}}} = \boldsymbol{\Sigma}_{\overline{ll}} - \mathbf{A}\boldsymbol{\Sigma}_{\hat{p}\hat{p}}\mathbf{A}^T. \tag{20}$$

following the usual derivations of a GMM [18]. Resubstituting these residuals leads to [18]:

$$\hat{\mathbf{v}} = \boldsymbol{\Sigma}_{ll}\mathbf{B}^T\boldsymbol{\Sigma}_{\overline{ll}}^{-1}\hat{\overline{\mathbf{v}}}. \tag{21}$$

These residuals are used to update the observations by $\mathbf{l}+\hat{\mathbf{v}}$ again to build up the Jacobian matrices of eq. (12) and to calculate the discrepancies of eq. (13). These transformations are performed in each iteration.

3 Analyzing biased estimates

Based on the least-squares estimation presented in the previous section, several simulated laser scans are approximated. Here, as already written, the station of the laser scanner changes between five positions while the position of the scanned plane remains fixed in the global coordinate system $[X, Y, Z]$. Furthermore, deformations with a magnitude of 5 mm are integrated in the plane (see Figure 3). These deformations vary regarding their spatial expansions. Either no deformation, one deformation – the one centered at the projection of station no. 1 – or four deformations are introduced.

Based on these different configurations, one simulated realization of observations is processed and analyzed each time. Due to the noising of the observations in each realization, the resulting estimates depend on the specific generated noise. However, the variation of the estimates due to this noise is negligible compared to the varying bias caused by network configuration and deformation. Thus, it can be disregarded. In the following, the results are illustrated and analyzed.

3.1 Results of parameter estimation

As three versions of planes – no, one or four deformations – and five different stations are processed, fifteen sets of parameters $\hat{\mathbf{p}} = [\hat{\bar{n}}_x, \hat{\bar{n}}_y, \hat{\bar{n}}_z]^T$ are estimated. These are transformed back into $\hat{\mathbf{p}}_4 = [\hat{n}_x, \hat{n}_y, \hat{n}_z, \hat{d}]^T$ using eq. (2) and afterwards into the global coordinate system so that they are comparable. The resulting parameters are $\hat{\mathbf{p}}_{\text{glo}} = [\hat{n}_X, \hat{n}_Y, \hat{n}_Z, \hat{D}]^T$. As the expressiveness of the dimensionless normal vector $[\hat{n}_X, \hat{n}_Y, \hat{n}_Z]^T$ is limited, it is transformed to the polar coordinates vertical angle $\hat{\Theta}$ and horizontal angle $\hat{\Phi}$ indicating the orientation of the estimated plane in the global coordinate system:

$$\hat{\Theta} = \arccos\left(\frac{\hat{n}_Z}{\sqrt{\hat{n}_X^2 + \hat{n}_Y^2 + \hat{n}_Z^2}}\right) \tag{22}$$

$$\hat{\Phi} = \arctan\left(\frac{\hat{n}_Y}{\hat{n}_X}\right). \tag{23}$$

Consequently, the two polar coordinates $\hat{\Theta}$ and $\hat{\Phi}$ as well as the distance $\hat{D}$ are analyzed in the final parameter vector $\hat{\mathbf{p}}_{\text{fin}} = [\hat{\Theta}, \hat{\Phi}, \hat{D}]^T$. Their deviations to the true values $\mathbf{p}_{\text{fin}}$ – known by eq. (5) – are shown in Figure 5. They are analyzed by a parameter significance test based on the test value

$$T = \frac{1}{h}\left(\hat{\mathbf{p}}_{\text{fin}} - \mathbf{p}_{\text{fin}}\right)^T \boldsymbol{\Sigma}_{\text{fin}}^{-1}\left(\hat{\mathbf{p}}_{\text{fin}} - \mathbf{p}_{\text{fin}}\right) \sim \mathcal{F} \tag{24}$$

where $\mathcal{F}$ indicates that T is Fisher-distributed. For $T \leq f_{h,r,1-\alpha}$, the difference between the estimates and the expectation values is insignificant [12]. This test depends on the significance level $\alpha = 1\%$, on the adjustment's redundancy r (eq. 26) and on the number of tested parameters $h = 3$ – resulting in the quantil $f_{h,r,1-\alpha}$ of the Fisher-distribution. The completely filled covariance matrix of the estimated parameters $\boldsymbol{\Sigma}_{\text{fin}}$ is gained by a three-step variance propagation from $\hat{\mathbf{p}}$ to $\hat{\mathbf{p}}_4$, then to $\hat{\mathbf{p}}_{\text{glo}}$ and finally to $\hat{\mathbf{p}}_{\text{fin}}$.

In Figure 5 can be seen that the estimated parameters indeed vary between the different laser scanner stations if deformations exist on the scanned surface. If no deformation exists, the variations are negligible and appear only due to the specific simulated realization of the stochastic process. Consequently, the significance test is accepted most times.

The bias of the estimated vertical angle and the distance based on the plane being deformed by only one deformation increases when the distance between scanner and deformation decreases (station no. 1 and 4, see Figure 3). This is expectable since the sampling density is greater at the deformation in these cases (see Figure 4). The horizontal angle is only biased by a smaller magnitude which is due to the dimension of the plane being four times longer in horizontal than in vertical direction. Thus, the ratio of deformed sampling points is four times higher in vertical direction.

Regarding the estimates when the plane is deformed four times, the results of varying biases are comparable.

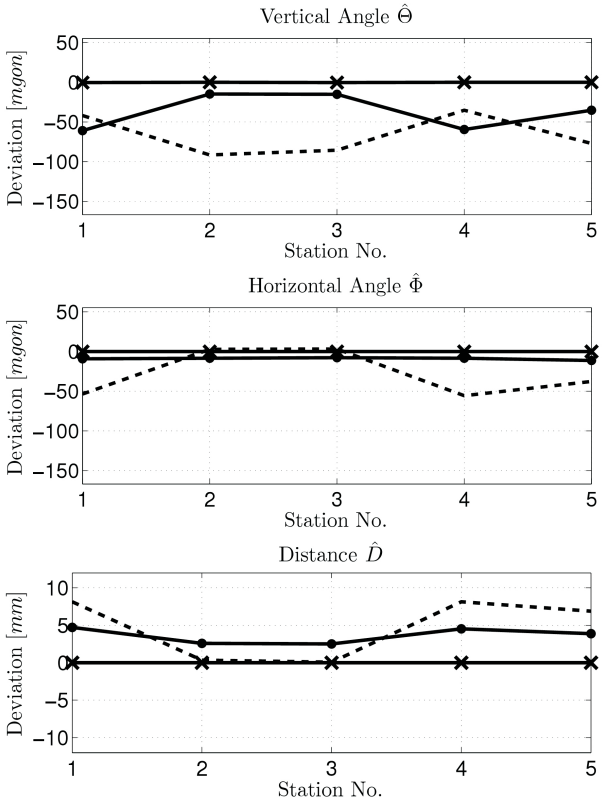

Fig. 5. Estimated global plane parameters of original adjustment; no deformation (crosses), one deformation (dots), four deformations (dashed).

The variation is even larger due to the existence of more deformed parts of the surface. This also holds for the horizontal angles as the deformations are now also distributed more in horizontal direction. Furthermore, due to the fact that not only one deformation exists, the position of maximal bias varies between the parameters and stations.

3.2 Analyzing the network configuration

Partial redundancies describe the controllability and the reliability of each observation [9]. These partial redundancies r_j can be calculated for each observation $l_j, j = 1, \ldots, n$, used in the GHM. Similarly, they can be calculated for the substituted observations $\bar{l}_i$ used in the GMM – thus, representing the controllability of a whole observation triplet $[s_i, \beta_i, t_i]^T$ or sampling point $[x_i, y_i, z_i]^T$, respectively:

$$\bar{r}_i = \left[\boldsymbol{\Sigma}_{\hat{\bar{v}}\hat{\bar{v}}}\boldsymbol{\Sigma}_{\bar{l}\bar{l}}^{-1}\right]_{i,i}; \qquad i = 1, \ldots, m. \tag{25}$$

Both values are related by $\bar{r}_i = r_{i,s} + r_{i,\beta} + r_{i,t}$. Since the sampling points' reliabilities are of interest, only $\bar{r}_i$ are investigated further.

Generally, partial redundancies – lying in the interval of [0, 1] for uncorrelated observations – depend on three different aspects:

1. the varying sampling density that is contained in **A** and **B** and, thus, in $\boldsymbol{\Sigma}_{\hat{v}\hat{v}}$ and $\boldsymbol{\Sigma}_{\hat{\bar{v}}\hat{\bar{v}}}$ (eq. 20),
2. the object's geometry, also contained in **A** and **B** and, thus, in $\boldsymbol{\Sigma}_{\hat{v}\hat{v}}$ and $\boldsymbol{\Sigma}_{\hat{\bar{v}}\hat{\bar{v}}}$ and
3. the observations' stochastic model equaling $\boldsymbol{\Sigma}_{ll}$ and $\boldsymbol{\Sigma}_{\bar{l}\bar{l}}$.

Thus, changing one of these aspects leads to a modification of the partial redundancies. As they imply the reliability of each observation, the modification of the partial redundancies leads to a change of the estimated parameters [9].

The partial redundancies of the plane approximation with the laser scanner being stationed at positions no. 1 and 3 are shown in Figure 6. As can be seen, the partial redundancies vary between both figures. This is due to the already described three effects of (1.) sampling density, (2.) object's geometry and (3.) stochastic model:

1. The trend of the partial redundancies is not strictly symmetric to the plane's center. This is because of the inhomogeneous sampling density resulting from the laser scanner not being positioned in front of the plane's center. The partial redundancy is higher in sections with dense point sampling.
2. The partial redundancies decrease when moving from the plane's middle to the endings. This phenomenon is well known as the points near the endings of the plane become more important [2]. Thus, this effect is due to the sampled object's geometry.
3. As the points' standard deviations increase porportionally to the measured distance (see Figure 2), the partial redundancies are higher when increasing the distance to the scanner. However, this effect is smaller and, thus, overlayed by the other two effects. It will get more visible after the proposed least-squares manipulations (see Figure 8).

These spatial distributions of the partial redundancies implicitly weight each sampling point in the adjustment. As this weight obviously depends on the scanning geometry, the parameters are biased and not reproducible when altering this scanning geometry. This explains the results of the approximation shown in Figure 5.

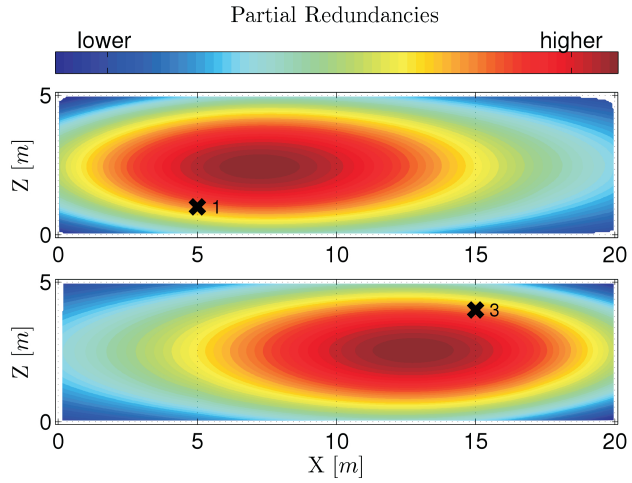

Fig. 6. Partial redundancies of the plane estimation from stations no. 1 (top) and no. 3 (bottom, both projected in XZ-plane); original adjustment.

The variation of the partial redundancies is only very small. This rests upon the fact that their sum equals the redundance of the adjustment

$$r = m - u = \sum_i \bar{r}_i = \sum_j r_j \tag{26}$$

As $m \approx 250,000$ is many times higher than u, the redundancy is approximately $r \approx m$. Thus, the partial redundancies $\bar{r}_i$ are all near their maximal value of 1. In the present case, they vary only by $\max(\bar{r}_i) - \min(\bar{r}_i) \approx 2 \cdot 10^{-5}$.

This small variation is typical when approximating laser scans since the number of parameters is always many times smaller than the number of observations. However, neither the actual magnitude of the partial redundancies nor the magnitude of their variation is of primary interest. Rather the spatial distribution of the partial redundancies' variation in the point cloud should be focused as it implies the diverging importance of the sampling points for parameter estimation.

4 Improvement by least-squares manipulation

As shown in the previous section, the parameter estimates are biased and non-reproducible. The present section introduces three different approaches for handling these effects. They aim at changing the sampling density (data reduction), the stochastic model (insertion of spatial correlations) or the impact of the object's geometry (balanced adjustment) to modify the partial redundancies and, hence, the estimates. After inroducing these algorithms, the parameter estimates are discussed.

4.1 Data reduction

Point clouds of laser scanners are often reduced to save processing time due to the highly redundant information [20, 21, 26, 32, 43]. Only seldom, the reduction is motivated by optimizing the sampling density regarding the network configuration [15]. However, this is the reason for reducing the data in the present case: the idea is to homogenize the partial redundancies so that their spatial distribution is more independent from the original scanning geometry.

For data reduction, three different types exist: (1.) uniform, (2.) curvature and (3.) random reduction [43]. As the aim is to increase the reproducibility of the estimation, only the first two approaches are relevant. The curvature based reduction reduces the point density depending on local object curvature, the uniform one grids the sampling points [20, 21, 26]. Thus, both are similar regarding the present case of approximating the point cloud to a plane that is not curved.

The implemented data reduction builds a nearly regular grid of observations maintaining as many observations as possible. No interpolation or other manipulation of specific observations is performed but an elimination of several observations due to their spatial position. This data reduction contains three steps:

1. finding the longest distance l_{dist} of neighbored points,
2. building a regular three-dimensional grid of cell length l_{dist} aligned to the point cloud's principal components, and
3. eliminating all points in each cell except for the one nearest to the cell middle.

Performing this reduction scheme, a nearly homogeneous sampling density originates. When scanning, e.g., from station no. 1, approximately 35,000 observations of the original 250,000 observations remain.

4.2 Insertion of spatial correlations

Usually, spatial correlations are integrated in the analysis of laser scans to cope either with surface-based systematic errors or with geometry-based systematic errors [16, 33, 36]. The first category would include, e.g., material reflection or penetration into the surface structure. The

second one would contain, e.g., laser beamwidth or incidence angles.

However, spatial correlations can also be introduced to change the network configuration. Spatial correlations of constant radii would consider in a similiar way to the data reduction that the sampling density is very inhomogeneous as the independence of dense distributed observations is decreased. Hence, not the number of points is reduced as in the data reduction but each individual point's impact on the parameter estimation.

By defining the magnitude of correlation by a Gaußian distribution curve with the parameter l_{corr} equaling the standard deviation, the correlation matrix $\mathbf{R}$ [18] with its elements $R_{i,j}(i, j = 1, \ldots, m)$ can be built up:

$$R_{i,j} = \exp\left(-\frac{1}{2}\left(\frac{D_{i,j}}{l_{\text{corr}}}\right)^2\right). \tag{27}$$

Here, $D_{i,j}$ equals the distance between sampling points i and j. The parameter l_{corr} is quantified regarding the cell length l_{dist} of the data reduction: $l_{\text{corr}} = l_{\text{dist}}/3$. Following probability theory [18], the triple of l_{corr}, i.e., l_{dist}, approximately equals the radius of correlation.

These correlations are integrated into the adjustment by adding them to the existing covariance matrix of the substituted observations $\boldsymbol{\Sigma}_{\overline{ll}}$ that originally equals a main diagonal matrix:

$$\boldsymbol{\Sigma}_{\overline{ll},\text{corr}} = \boldsymbol{\Sigma}_{\overline{ll}} + (0.9 \cdot (\mathbf{R} - \mathbf{I})) \circ \left(\overline{\boldsymbol{\sigma}}_{ij}\overline{\boldsymbol{\sigma}}_{ij}^T\right), \tag{28}$$

with $\overline{\boldsymbol{\sigma}}_{ij} = \sqrt{\text{diag}\left(\boldsymbol{\Sigma}_{\overline{ll}}\right)}$ [42]. The minimization of $\mathbf{R}$ by the identity matrix $\mathbf{I}$ considers that the main diagonal should not be altered, the factor 0.9 scales all correlations to avoid instability in the adjustment due to nearly full correlated measurements.

Subsequently, the estimation of Sec. 2 is manipulated in the way that the covariance matrix $\boldsymbol{\Sigma}_{\overline{ll},\text{corr}}$ is incorporated into eqs. (17-21) instead of $\boldsymbol{\Sigma}_{\overline{ll}}$.

4.3 Balancing the adjustment

The sampled object's geometry impacts the least-squares parameter estimation. This has already been known since, e.g., high-leverage points are analyzed: these points impact parameter estimations by a high ratio only due to their position on the object [2]. To eliminate the impact of the sampled object's geometry, the adjustment can be balanced [25].

For balancing an adjustment, balancing factors $\tilde{p}_{\text{bal},i}$ are used to weight each observation. These balancing factors arise out of the network configuration similar to the partial redundancies. But here, the so called normal form of the design matrix needs to be calculated since this normal form contains the desired geometrical information [25]. Therefore, u rows of the design matrix $\mathbf{A}$ of arbitrary index are extracted to build up a matrix $\mathbf{W}$. The normal form of $\mathbf{A}$ afterwards follows by $\overline{\mathbf{A}} = \mathbf{A}\mathbf{W}^{-1}$.

Using the normal form $\overline{\mathbf{A}}$, the balancing factors $\tilde{p}_{\text{bal},i}$ are iteratively estimated [25] to afterwards update the covariance matrix of the observations:

$$\boldsymbol{\Sigma}_{\overline{ll},\text{bal}} = \boldsymbol{\Sigma}_{\overline{ll}} \cdot \begin{bmatrix} \tilde{p}_{\text{bal},1} & & \\ & \ddots & \\ & & \tilde{p}_{\text{bal},m} \end{bmatrix}^{-1}. \tag{29}$$

In the end, this covariance matrix $\boldsymbol{\Sigma}_{\overline{ll},\text{bal}}$ is incorporated into eqs. (17-21) instead of $\boldsymbol{\Sigma}_{\overline{ll}}$.

After balancing an adjustment, the influence of the object's geometry as well as the one of the sampling density is eliminated. This leads to partial redundancies that would all be equal if the observational variances were identical and uncorrelated. However, as this is not the case in the present application, the partial redundancies nearly solely depend on the stochastic model.

As already written, the submatrix $\mathbf{W}$ consists of u chosen rows of $\mathbf{A}$. These chosen rows should not correspond to neighboured sampling points when scanning with high resolution. Otherwise, the calculation of the normal form could be bad conditioned as $\mathbf{W}$ is numerically nearly rank defficient.

4.4 Results and analysis of parameter estimation

The parameter estimates based on the simulation of the different stations are given in Figure 7. This time, only the results regarding the inclusion of all four deformations are inspected. As can be seen, the reproducibility of the estimates can be increased in all three components when reducing the data or inserting spatial correlations. The results of these two manipulations do not differ significantly from each other. Contrary, the estimates of the balanced adjustment decrease the reproducibility compared to the original adjustment. The biases are not reduced significantly in all of these manipulations, also indicated by the declined significance tests.

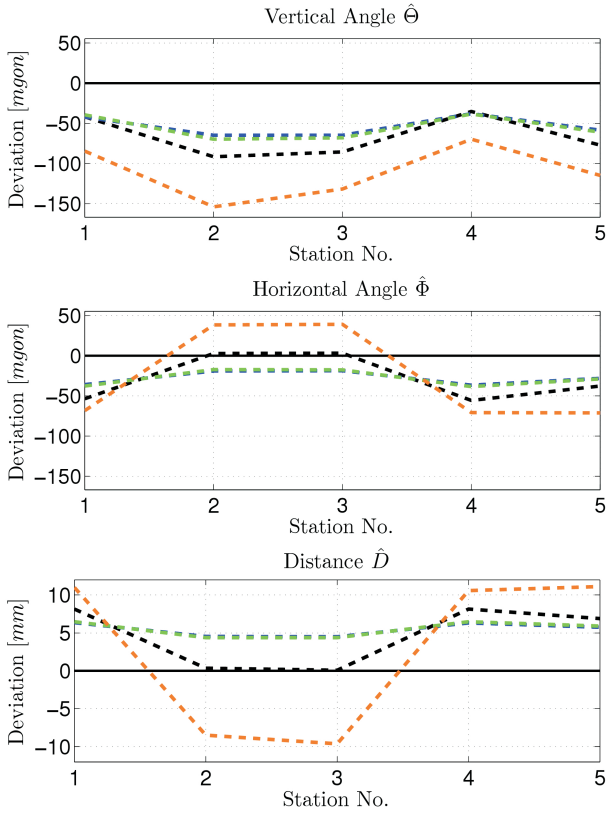

Fig. 7. Estimated global plane parameters of deformed plane based on least-squares manipulations; data reduction (blue), insertion of correlations (green), balanced adjustment (brown), original adjustment (black).

be reduced. This can also be seen in the partial redundancies as the impact of the deformation is not decreased.

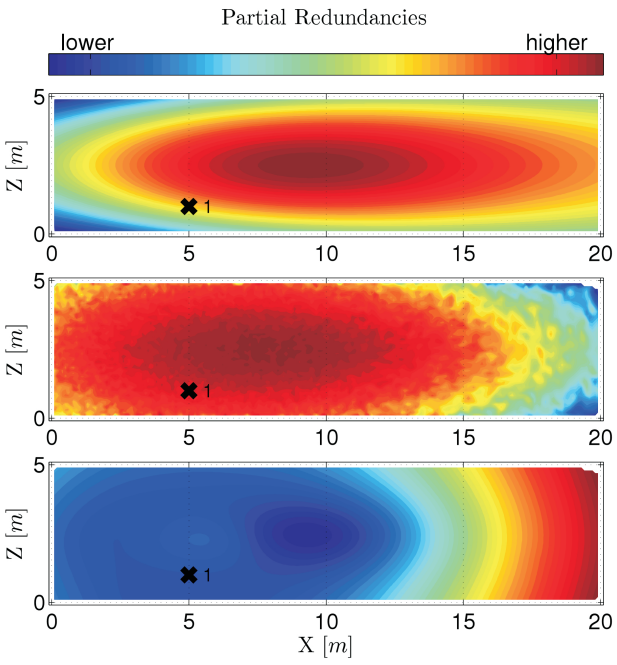

Fig. 8. Partial redundancies of the plane estimation from station no. 1 (cross, projected in XZ-plane); data reduction (top), insertion of correlations (middle), balanced adjustment (bottom).

Data reduction

The partial redundancies of the reduced data show that the impact of the sampling density is eliminated (Figure 8). The position of maximal partial redundancy is almost in the middle of the plane due to the increased impact of the object's geometry now. Furthermore, by investigating that the partial redundancies are not strictly symmetric but higher on the right side of the plane, the impact of the stochastic model is visible more clearly than in the original adjustment. This is because the point accuracy is less on the right side due to the longer distances to the scanner station. Nevertheless, the most important fact is that the impact of the sampling density is eliminated.

As the sampling density impacts the network configuration the most, the reproducibility can be increased significantly even when scanning deformed surfaces. The influence of the deformations is homogenized as the number of points positioned on the deformations does not depend on the original scanning geometry. However, the bias cannot

Insertion of spatial correlations

Regarding the partial redundancies of the correlated adjustment (Figure 8), it can be seen that the trend of the spatial distribution is similiar to the original adjustment. But deviating, the systematic seems to be mitigated as the variation of the partial redundancies is decreased. Furthermore, – what cannot be seen in Figure 8 – the partial redundancies are not in the interval of [0, 1] anymore due to the sampling points' correlations. However, the impact of correlating the adjustment is not as clearly visible as is the case at the other two least-squares manipulations.

Disregarding this fact, the effect of inserting spatial correlations is very similiar to the data reduction. This is expectable since the radius of spatial correlation is chosen corresponding to the point distance after data reduction. Hence, the bias cannot be reduced in all estimates but the reproducibility is improved.

Balancing the adjustment

The partial redundancies of the balanced adjustment show that the impact of the object's geometry as well as the one of the sampling density are indeed eliminated (Figure 8). The remaining structure is nearly only due to the stochastic model since the distribution of the partial redundancies is similiar to the one of the sampling points' total standard deviations (see Figure 2).

This effect causes even more biased and less reproducible results. Thus, the opposite of the desired effect is achieved. This is expectable when combining Figure 4 and Figure 8: in the original adjustment, a locally higher sampling density results in higher partial redundancies. As the effect of the sampling density on the partial redundancies is eliminated by balancing the adjustment, only the stochastic model rules about the network configuration. Thus, the partial redundancies are lower at high sampling densities as the sampling density is high near the scanner where the sampling points' standard deviations are lower. Consequently, areas near the scanner are weighted twice by the balanced adjustment: by the high sampling density as well as by the balancing factors.

5 Improvement by robust estimation

The results of the previous section show that the reproducibility can be increased significantly when reducing the data or introducing spatial correlations. However, the estimates are still biased. Therefore, it is of interest whether other techniques – besides the usual least-squares adjustment – yield better results.

Robust estimation techniques are usually used to approximate data by some model where the data is affected by gross errors [1, 37, 42]. The impact of gross errors is less in robust estimation than in usual least-squares estimation. Thus, it should be investigated if robust estimation is also suited for approximating data where the functional model is affected by systematic errors, i.e., local deformations. As representative for robust estimation, the RANSAC-algorithm (Random Sample Consensus) and the BIBER-estimator (Bounded Influence By Standardized Residuals) are investigated. After introducing the two methods, the results regarding the already discussed examples are presented.

5.1 BIBER-estimator

The BIBER-estimator belongs to the family of modified M-estimators [40, 41]. These types of estimators are more robust than a classical least-squares approach because outliers do impact the estimation less: in a classical least-squares adjustment, e.g., the GHM or GMM, the cost function $\mathbf{v}^T\mathbf{v}$ is minimized (see Sec. 2), disregarding the covariance matrix $\boldsymbol{\Sigma}_{ll}$. Thus, the square sum of the residuals $\mathbf{v}$ is minimized. If outliers having large residuals exist, they influence the minimization of the cost function. At (modified) M-estimators, the influence of outliers is restricted by not minimizing the square sum of the corresponding residuals. This can be done by weighting the observations dependent on their residual [17, 19].

Modified M-estimators – in contrast to usual M-estimators – incorporate not only the residuals of the observations in the weight but also their reliability due to the network configuration. At the BIBER-estimator, this results in weighting each observation if its standardized residual

$$\hat{\omega}_i = \frac{\hat{\bar{v}}_i}{\hat{\sigma}_{\bar{v},i}} = \frac{\hat{\bar{v}}_i}{\sigma_{\bar{l},i} \cdot \sqrt{\bar{r}_i}}, \tag{30}$$

where $\hat{\sigma}^2_{\bar{v},i} = [\boldsymbol{\Sigma}_{\hat{\bar{v}}\hat{\bar{v}}}]_{i,i}$, outnumbers a threshold c [40, 41]:

$$p_{\mathrm{BIBER},i} = \begin{cases} 1 & |\hat{\omega}_i| < c \\ c/|\hat{\omega}_i| & |\hat{\omega}_i| \geq c \end{cases}. \tag{31}$$

Thus, standardized residuals smaller than the threshold c are not weighted so that they are minimized as in the least-squares estimation. The other ones are weighed down so that they impact the estimation less. The threshold c is usually set up in the interval $[2.5, 4]$ [40]; here, it equals 2.58 related to an outlier test with 99.0% confidence level [29].

As these weights are based on the estimated residuals of eq. (19), they cannot be integrated before the second iteration step. To gain a more stable estimation, the weights are scaled to a total number of m by $\tilde{p}_{\mathrm{BIBER},i} = p_{\mathrm{BIBER},i} / \sum p_{\mathrm{BIBER},i} \cdot m$ similar to the balancing factors. Based on this, the covariance matrix

$$\boldsymbol{\Sigma}_{\bar{l}\bar{l},\mathrm{BIBER}} = \boldsymbol{\Sigma}_{\bar{l}\bar{l}} \cdot \begin{bmatrix} \tilde{p}_{\mathrm{BIBER},1} & & \\ & \ddots & \\ & & \tilde{p}_{\mathrm{BIBER},m} \end{bmatrix}^{-1} \tag{32}$$

is incorporated into eqs. (17-21) instead of $\boldsymbol{\Sigma}_{\bar{l}\bar{l}}$.

5.2 RANSAC-algorithm

The RANSAC-algorithm was developed to fit a model to data containing a significant percentage of outliers [5, 8,

37]. It is based upon not using all observations for estimating the desired parameters but upon only using the least number of observations that is possible. By selecting different samples of observations very often, the parameters are calculated many times. Then, out of these parameter sets, the best one is chosen. Hence, the RANSAC-algorithm is no adjustment minimizing all residuals in some way as are the other presented algorithms – least-squares as well as robust. Following, the parameter significance test as proposed in eq. (24) cannot be performed.

The implementation of the RANSAC-algorithm is as follows [4]:

1. Selection of 3 randomly chosen sampling points. No triple can be selected twice and at least two points need to have a distance of minimial 5 meters to each other.
2. Estimation of the plane parameters as described in Sec. 2 based on these 3 points. As 3 points contain 9 observations but only 3 parameters are calculated, this implementation also leads to a redundant adjustment.
3. Calculation of a consensus set. This equals a selection of all sampling points that do fit to the estimated plane model. A sampling point does not fit to the model if its deviation from the model

$$|\hat{\bar{n}}_x \cdot x_i + \hat{\bar{n}}_y \cdot y_i + \hat{\bar{n}}_z \cdot z_i - 1| \tag{33}$$

is greater than its standard deviation $\sigma_{xyz,i}$ (eq. 9).

These steps are processed 10, 000-times. This magnitude is chosen by empirical investigations; a further enhancement of this magnitude does not improve the results significantly anymore. The finally chosen parameter solution equals the one being supported by the most sampling points, i.e., the one having the largest consensus set.

5.3 Results and analysis of parameter estimation

The results of parameter estimation are shown in Figure 9. Comparing to the original adjustment and even comparing to the least-squares manipulations, the reproducibility and the unbiasedness can be improved significantly. This holds for the BIBER-estimator as well as for the RANSAC-algorithm. However, the significance test that can be performed for the BIBER-estimator still indicates deviations that do significantly deviate from the true values. Consequently, the estimates still depend on the scanning geometry – even though less than at the least-squares estimations.

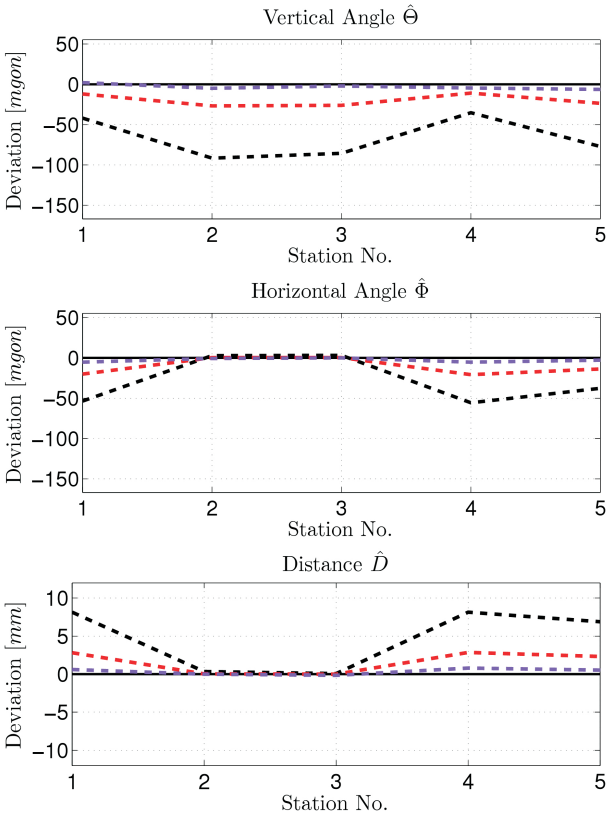

Fig. 9. Estimated global plane parameters of deformed plane based on robust adjustments; BIBER-estimator (red), RANSAC-algorithm (purple), original adjustment (black).

BIBER-estimator

For the BIBER-estimator, the partial redundancies are shown in Figure 10. They are calculated similarly to the least-squares estimations (eq. 25), this time incorporating the modified covariance matrix $\boldsymbol{\Sigma}_{\overline{ll},\mathrm{BIBER}}$ affecting $\boldsymbol{\Sigma}_{\hat{\bar{v}}\hat{\bar{v}}}$ and, thus, $\bar{r}_i$ [40].

The partial redundacies now consist of two systematics: (1.) the first one is similar to the one of the partial redundancies of the original adjustment (see Figure 6). Here, the corresponding sampling points' standardized residuals are smaller than the threshold – thus, they are not treated as outliers. (2.) The second systematic enlarges the partial redundancies of the sampling points being affected by the local deformations – these observations are weighted down due to high standardized residuals implying that the observations are outliers. Thus, the impact of

the observations on the parameter estimation depends on the network configuration as well as on their residuals.

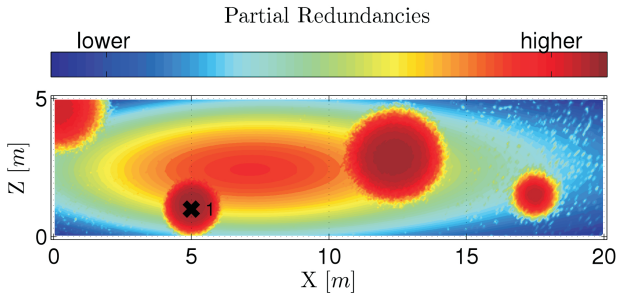

Fig. 10. Partial redundancies of the plane estimation from station no. 1 (cross, projected in XZ-plane); BIBER-estimator.

justment degrades the results. Robust techniques, i.e., the BIBER-estimator and the RANSAC-algorithm, improve the reproducibility as well as the unbiasedness in this case; the RANSAC-algorithm seems to be the best solution. However, as can be seen in Table 3, the RANSAC-algorithm is the worst estimator of the discussed ones when no deformation exists.

Hence, a combined strategy could be suited. This strategy would aim at eliminating the systematic error in the functional model, i.e., the local deformations, in three steps:

1. robust estimation by the RANSAC-algorithm,
2. detection of deformations and elimination of corresponding sampling points, and
3. least-squares estimation.

RANSAC-algorithm

As the RANSAC-algorithm calculates the parameters many times – but each time only based upon three sampling points – the partial redundancies cannot be analyzed. However, the increase of the unbiasedness can be explained by the number of points being influenced by the local deformations. As this number is small compared to the total number of sampling points, the consesus of all estimated plane parameters is larger near the true, undeformed plane. Apparently, the proportion of the points not being influenced by the local deformations is higher than the breakdown point of this robust adjustment [37].

The cruicial step would be part (2.) as it is to judge whether sampling points are influenced by a deformation or not. If the deformed parts could reliably be detetected in this step (2.), the following estimates of step (3.) would not be biased due to a functional model not suffering from any systematic error. Additionally, they would be optimal due to the least-squares minimization.

A simple implementation of these three steps has been performed leading to the results also shown in Tables 2–3. Here, the eliminated sampling points are the ones not being integrated in the consensus set. Thus, plotting the partial redundancies would equal Figure 6 with gaps at the four deformations. As expected, the results are always better than the ones of the RANSAC-algorithm. Nevertheless, the deformed parts of the simulated plane are quite easy to detect in part (2.). Hence, before transfering this specific result to general applications, it should be analyzed further.

6 Discussion and resulting suggestion

The results of the previous sections show that unlimited unbiasedness and reproducibility cannot be achieved by any of the discussed least-squares or robust estimations. Table 2 and Table 3 quantify these results. Table 2 corresponds to the plane being deformed four times. These results have already been examined deeper in the previous sections (see Figure 5, Figure 7 and Figure 9). The results of Table 3 are the ones corresponding to the plane not being deformed; they have not been discussed before except for the original adjustment (Figure 5).

Based on these tables, it can be stated that the insertion of correlations and the data reduction both produce similar results – they improve the reproducibility if unknown deformations exist. Contrary, balancing the ad-

7 Conclusion and outlook

The present study analyzes estimates based on laser scans of surfaces with unknown deformations. It is investigated how the adjustment's network configuration impacts the parameter estimation. Here, the sampling density, the object's geometry as well as the stochastic model are the relevant aspects. It is pointed out that the estimates are biased and not reproducible if deformations equaling systematic errors in the functional model exist. These investigations have not been done before regarding the literature. Following, the estimates of surfaces based on laser scans pro-

Table 2. Including four deformations in plane: bias and reproducibility of all estimates (vertical angle $\hat{\Theta}$, horizontal angle $\hat{\Phi}$, distance $\hat{D}$) of the different adjustments (ls=least-squares, r=robust).

Adjustment	Type	Bias			Reproducibility		
		$\hat{\Theta}$[mgon]	$\hat{\Phi}$ [mgon]	$\hat{D}$ [mm]	$\hat{\Theta}$ [mgon]	$\hat{\Phi}$ [mgon]	$\hat{D}$ [mm]
Original adjustment	ls	-66.0	-28.1	4.7	55.7	58.7	8.1
Data reduction	ls	-53.1	-27.6	5.5	28.4	17.6	1.8
Insertion of spatial correlations	ls	-55.3	-27.9	5.5	31.4	21.0	2.1
Balancing the adjustment	ls	-110.7	-26.5	2.9	83.8	110.0	20.7
BIBER-estimator	r	-19.7	-10.6	1.6	15.8	21.2	2.8
RANSAC-algorithm	r	-3.1	-2.7	0.4	8.6	5.2	0.9
Elimination of systematic error	r+ls	-1.4	-2.4	0.3	4.2	4.5	0.6

Table 3. Including no deformation in plane: bias and reproducibility of all estimates (vertical angle $\hat{\Theta}$, horizontal angle $\hat{\Phi}$, distance $\hat{D}$) of the different adjustments (ls=least-squares, r=robust).

Adjustment	Type	Bias			Reproducibility		
		$\hat{\Theta}$ [mgon]	$\hat{\Phi}$ [mgon]	$\hat{D}$ [mm]	$\hat{\Theta}$ [mgon]	$\hat{\Phi}$ [mgon]	$\hat{D}$ [mm]
Original adjustment	ls	-0.1	0.0	0.0	0.2	0.1	0.0
Data reduction	ls	-0.2	0.0	0.0	0.6	0.3	0.0
Insertion of spatial correlations	ls	0.0	0.0	0.0	0.2	0.1	0.0
Balancing the adjustment	ls	-0.1	0.0	0.0	0.3	0.1	0.0
BIBER-estimator	r	-0.1	0.0	0.0	0.2	0.1	0.0
RANSAC-algorithm	r	-0.8	-0.2	0.1	5.2	1.3	0.3
Elimination of systematic error	r+ls	-0.2	-0.1	0.0	0.7	0.3	0.0

posed in miscellaneous publications are possibly biased and non-reproducible.

The least-squares estimates can be improved regarding the reproducibility by data reduction or insertion of spatial correlations. However, the bias cannot be eliminated. Contrary, robust adjustments as the BIBER-estimator or the RANSAC-algorithm can either increase the reproducibility as well as the unbiasedness. Nevertheless, – as robust adjustments are not a least-squares minimization – they do not minimize the residuals of the observations optimally. The better solution could be a combined approach of eliminating the systematic error resulting in improved estimates in the present case.

While these investigations are only shown here by approximating locally deformed planes, the formulated problem statement and the presented analysis can be transferred to other applications, objects and configurations. Investigations of simulated and real data either have already been shown [15] or will be in further studies, e.g., regarding the approximation of paraboloids [13, 16]. Consequently, to guarantee reproducible and unbiased estimates even when scanning surfaces containing local, unknown and, thus, non-parameterized deformations, the presented analysis and its solutions should be investigated further.

Acknowledgement: The writers thank the anonymous reviewers for their valuable comments and suggestions that helped to significantly improve the quality of the paper.

References

[1] Borutta H., *Robuste Schätzverfahren für geodätische Anwendungen*, Ph.D. thesis, Studiengang Vermessungswesen, Universität der Bundeswehr München, no. 33, 1988.

[2] Chatterjee S. and Hadi A. S., Influential observations, high leverage points, and outliers in linear regression, *Stat. Sci.* 1 (1986), 379–416.

[3] Chmelina K., Jansa J., Hesina G. and Traxler C., A 3-d laser scanning system and scan data processing method for the monitoring of tunnel deformations, *J. Appl. Geodesy* 6 (2012), 177–185.

[4] Choi S., Kim T. and Yu W., Performance evaluation of RANSAC family, *BMVC* 81 (2009), 1–12.

[5] Chum O., *Two-view geometry estimation by random sample and consensus*, Ph.D. thesis, Center for Machine Perception, Czech Technical University in Prague, 2005.

[6] Cothren J. D., *Reliability in constrained Gauss-Markov models: an analytical and differential approach with applications in photogrammetry*, Ph.D. thesis, Ohio State University, 2004.

[7] Eling D., *Terrestrisches Laserscanning für die Bauwerksüberwachung*, Ph.D. thesis, Wissenschaftliche Arbeiten der Fachrichtung Geodäsie und Geoinformatik der Leibniz Universität Hannover, no. 282, 2009.

[8] Fischler M. A. and Bolles R. C., Random sample consensus: a paradigm for model fitting with applications to image analysis and automated cartography, *Communications of the ACM* 24 (1981), 381–395.
[9] Förstner W., Reliability analysis of parameter estimation in linear models with applications to mensuration problems in computer vision, *Comput. Vision. Graph.* 40 (1987), 273–310.
[10] Gordon S. J. and Lichti D. D., Modeling terrestrial laser scanner data for precise structural deformation measurement, *J. Surv. Eng.* 133 (2007), 72–80.
[11] Grafarend E. W., *Optimization of design and computation of control networks, ch. Third-order design of geodetic networks*, pp. 133–149, Akadémiai Kiadó, Budapest, 1979.
[12] Heunecke O., Kuhlmann H., Welsch W., Eichhorn A. and Neuner H., Auswertung geodätischer Überwachungsmessungen, Handbuch Ingenieurgeodäsie (M. Möser, G. Müller and H. Schlemmer, eds.), Wichmann, Heidelberg, 2nd ed, 2013.
[13] Holst C., Dupuis J., Paulus S. and Kuhlmann H., Flächenhafte Deformationsanalysen mit terrestrischen und Nahbereichslaserscannern - eine Gegenüberstellung anhand von Beispielen, *Allgem. Verm. Nachr.* 7 (2014).
[14] Holst C., Eling C. and Kuhlmann H., Automatic optimization of height network configurations for detection of surface deformations, *J. Appl. Geodesy* 7 (2013), 103–113.
[15] Holst C. and Kuhlmann H., *Impact of spatial point distributions at laser scanning on the approximation of deformed surfaces*, Ingenieurvermessung 14. Beiträge zum 17. Internationalen Ingenieurvermessungskurs, A. Wieser, Zurich, 2014, pp. 269–282.
[16] Holst C., Zeimetz P., Nothnagel A., Schauerte W. and Kuhlmann H., Estimation of focal length variations of a 100-m radio telescope's main reflector by laser scanner measurements, *J. Surv. Eng.* 138 (2012), 126–135.
[17] Huber P. J., Rboust estimation of a location parameter, *Ann. Math. Stat.* 36 (1964), 1753–1758.
[18] Koch K.-R., Parameter estimation and hypothesis testing in linear models, Springer, Berlin, Heidelberg, New York, 1987.
[19] Koch K.-R., Parameterschätzung und Hypothesentests, Dümmler, Bonn, 1997.
[20] Lee K. H., Woo H. and Suk T., Data reduction methods for reverse engineering, *Int. J. Adv. Manuf. Technol.* 17 (2001), 735–743.
[21] Lee K. H., Woo H. and Suk T., Point data reduction using 3D grids, *Int. J. Adv. Manuf. Technol.* 18 (2001), 201–210.
[22] Leica Geosystems, Leica HDS 6100, latest generation of ultra-high speed laser scanner., www.leica-geosystems.com/hds, May 2011.
[23] Lichti D. D., A resolution measure for terrestrial laser scanners, The International Archives of Photogrammetry, *Remote Sensing and Spatial Information Sciences* 34 (2004), 552–558.
[24] Lichti D. D. and Jamtsho S., Angular resolution of terrestrial laser scanners, *Photogramm. Rec.* 21 (2006), 141–160.
[25] Linke J., *Zur Analyse der Geometrie und Beurteilung von geodätischen und mechanischen Netzen unter Verwendung von Balancierungsfaktoren*, Ph.D. thesis, Institut für Geotechnik und Markscheidewesen der TU Clausthal, no. 3, 2000.
[26] Mandow A., Martinez J. L., Reina A. J. and Morales J., Fast range-independent spherical subsampling of 3D laser scanner points and data reduction performance evaluation for scene registration, *Pattern Recognit. Lett.* 31 (2011), 1239–1250.
[27] Mikhail E. M. and Ackermann F., *Observations and least squares*, Dun-Donelly, New York, 1976.
[28] Neitzel F. , Generalization of total least-squares on example of unweighted and weighted 2D similarity transformation, *J. Geod.* 84 (2010), 751–762.
[29] Niemeier W., *Ausgleichungsrechnung. Statistische Auswertemethoden*, 2nd ed, de Gruyter, Berlin, 2008.
[30] Pesci A., Teza G. and Bonali E., Terrstrial laser scanner resolution: numerical simulations and experiments on spatial sampling optimization, *Remote Sens.* 3 (2011), 167–184.
[31] Peternell M. , Developable surface fitting to point clouds, *Comput. Aided Geom. D.* 21 (2004), 785–803.
[32] Puttonen E., Lehtomäki M., Kaartinen H., Zhu L., Kukko A. and Jaakkola A., Improved sampling for terrestrial and mobile laser scanner point cloud data, *Remote Sens.* 5 (2013), 1754–1773.
[33] Schaer P., Skaloud J., Landtwing S. and Legat K., Accuracy estimation for laser point cloud including scanning geometry, in: *5th International Symposium on Mobile Mapping Technology*, Padua, Italy, 2007.
[34] Schäfer T., *Eine Simulationsumgebung zur Analyse berührungsloser Distanzmessungen unter Berücksichtigung der Interaktion zwischen Laserstrahl und Objekt*, Ingenieurvermessung 14. Beiträge zum 17. Internationalen Ingenieurvermessungskurs, A. Wieser, Zurich, 2014, pp. 27–36.
[35] Soudarissanane S., Lindenbergh R., Menenti M. and Teunissen P., Scanning geometry: influencing factor on the quality of terrestrial laser scanning points, *ISPRS J. Photogramm.* 66 (2011), 389–399.
[36] Sun X., Rosin R. L., Martin R. R. and Langbein F. C., Noise analysis and synthesis for 3D laser depth scanners, *Graph. Models* 71 (2009), 34–48.
[37] Torr P. H. S. and Murray D. W., The development and comparison of robust methods for estimating the fundamental matrix, *Int. J. Comput. Vision* 24 (1997), 271–300.
[38] Wang J., Kutterer H. and Fang X., On the detection of systematic errors in terrestrial laser scanning data, *J. Appl. Geodesy* 6 (2012), 187–192.
[39] Wendland H., Piecewise polynomial, positive definite and compactly supported radial functions of minimial degree, *Adv. Comput. Math.* 4 (1995), 389–396.
[40] Wicki F., *Robuste Schätzverfahren für die Parameterschätzung in geodätischen Netzen*, Ph.D. thesis, Institut für Geodäsie und Photogrammetrie and der Eidgenössischen Technischen Hochschule Zürich, 1999, no. 67.
[41] Wicki F., *Robust estimator for the adjustment of geodetic networks*, First International Symposium on Robust Statistics and Fuzzy Techniques in Geodesy and GIS (A. Carosio and H. Kutterer, eds.), Institut für Geodäsie und Photogrammetrie and der Eidgenössischen Technischen Hochschule Zürich, 2001, no. 295.
[42] Wieser A., *Robust and fuzzy techniques for parameter estimation and quality assessment in GPS*, Ph.D. thesis, TU Graz, Shaker, 2001.
[43] Zainuddin K., Setan H. and Majid Z., From laser point cloud to surface: data reduction procedure test, *Geoinformation Science Journal 9* (2009), 1–9.